#### Log Number: 256

## THE KELVIN-HELMHOLTZ INSTABILITY: COMPARISONS OF ONE- AND TWO-DIMENSIONAL SIMULATIONS

W. Fullmer, M. Lopez de Bertodano and V. H. Ransom
Purdue University, West Lafayette, IN USA
wfullmer@purdue.edu, bertodan@purdue.edu, ransom@ecn.purdue.edu

#### **Abstract**

A 1D two-fluid model for horizontal stratified flow is presented and discussed in the context of the Kelvin-Helmholtz instability. The model is well-posed because it includes surface tension. However, well-posedness is not sufficient. It is shown that non-linear stability (i.e., bounded wave growth) is also a necessary condition for convergence.

A turbulent viscosity is constituted for the 1D two-fluid model by means of 2D LES using the VOF piece-wise linear approach to track the interface. The 1D model Reynolds stress thus obtained is used to represent missing physics in 1D associated with viscous dissipation due to vorticity. With the added Reynolds stress the 1D numerical model exhibits bounded wave growth and it also converges.

#### 1. Introduction

The Inviscid Kelvin-Helmholtz (IKH) instability in horizontal stratified flow has been the subject of considerable research within the framework of the one-dimensional (1D) two-fluid model. It is of particular interest to the analysis of the stability of the model because it is an extreme case that produces high frequency waves that are amplified if the model is ill-posed. Taitel and Dukler [1] used linear stability theory to predict the flow regime transition from stratified to slug flow when the IKH instability occurs. In their simple interpretation the one-dimensional two-fluid model becomes ill-posed at the transition. However Ramshaw and Trapp [2] found that adding surface tension makes the model well-posed. Previously [5] it was shown through linear and nonlinear stability analyses that inclusion of surface tension into a 1D two-fluid model framework does render the model well-posed with a critical wavelength near the experimentally reported values. It was also shown that the model was capable of predicting the onset of the IKH instability which was benchmarked against 2D two-fluid model simulations as well as the experimental data of Thorpe [6]. Nevertheless the capillary waves grow unboundedly past the IKH instability point.

It has been shown by Kreiss and Yström [3] that the nonlinear behavior of a system of Burgers equations similar to the 1D two-fluid model with a small value of artificial viscosity results in dissipative shocks that limit the growth and amplitude of the waves. This theoretical result is significant because it shows that the amplitude of the waves in a two-fluid model with first order finite difference scheme is limited by the numerical viscosity. The shock steepening and formation is analogous to the wavelength cascading results reported by Krishnamurthy and Ransom [4]. They analyzed a toroidal stratified flow where a long wavelength disturbance was transferred to shorter wavelengths, until the energy was dissipated by numerical viscosity. They hypothesized that this process was similar to turbulent eddies cascading down to the

Kolmogorov length scale. However, numerical viscosity has several shortcomings: it is not based on physics and it varies with mesh size so that the numerical model does not converge.

The objective of the present work is to use a 2D computational fluid dynamics (CFD) simulation of high accuracy to constitute a Reynolds stress term for the 1D two-fluid model based on Kreiss and Yström's shocks [3]. Such a term should substitute missing physics (vorticity, wave breaking, etc.) so that the model does not have to rely on inaccurate numerical dissipation to limit the growth of the waves.

## 2. Description of Thorpe's experiment

The 1D and 2D numerical simulations are benchmarked against the experiments of S. A. Thorpe [6]. In the experiments a glass rectangular channel is filled with two immiscible fluids of different densities. The channel is 1.83m long, 3cm tall and 10cm wide which allows for quasi-2D waves. The fluids are water and commercial paraffin (kerosene) with carbon tetrachloride. The paraffin is used in place of air because its density is much closer to that of water. This decreases the acceleration of the fluids and extends the data collection time window. The properties of the fluids are:  $\rho_1 = 780 \text{ kg/m}^3$ ,  $\rho_2 = 1000 \text{ kg/m}^3$ ,  $\mu_1 = 0.0015 \text{ Pa}$  s,  $\mu_2 = 0.001 \text{ Pa}$  s and  $\sigma = 0.04 \text{ N/m}$ .

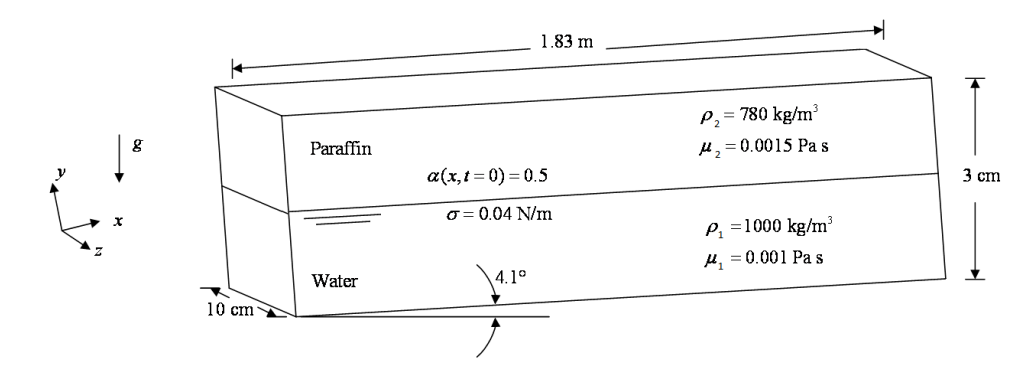


Figure 1 Experimental configuration and physical properties of Thorpe [6].

The channel is initially half filled with each fluid and allowed to settle in the horizontal position before one end was sharply raised. Video was taken of the counter-current accelerating fluids from above and on the side. The angle was varied from  $4 - 12^{\circ}$  in the experiments. In the simulations for which images have been published the angle is such that  $\sin \theta = 0.072$ . The time of the onset of instability was found to be  $1.88 \pm 0.07$ sec which includes half of the time to tilt the channel (about 0.25 sec). The measured value of the critical wavelength is 3.3 cm with  $\pm$  1 cm root mean square giving an uncertainty band of 2.4 - 4.4 cm.

### 3. One-dimensional model

The 1D two-fluid model [7] defines the conservation equations with the following simplifying assumptions: incompressible, isothermal, wall shear is generally neglected and the convective

covariance is unity. The resulting equations of mass and momentum in non-conservative form are:

$$\frac{\partial}{\partial t}\alpha_k \rho_k + \frac{\partial}{\partial x}\alpha_k \rho_k u_k = 0 , \qquad (1)$$

$$\alpha_k \rho_k \frac{\partial u_k}{\partial t} + \alpha_k \rho_k u_k \frac{\partial u_k}{\partial x} = -\alpha_k \frac{\partial P_k}{\partial x} + \frac{\partial}{\partial x} \alpha_k \rho_k \left( v_k \frac{\partial u_k}{\partial x} - u_k' u_k' \right) - \alpha_k \rho_k g_x + M_{ik} . \tag{2}$$

where k = 1, 2 correspond to kerosene and water respectively. The first term on the RHS is phasic pressure gradient which, in this form, represents the total force due to mean pressure, hydrostatic and surface tension effects. The second term on the RHS represents the viscous and Reynolds stresses and the last term represents the interfacial forces. All solution variables represent Reynolds averaged, area averaged and void weighted quantities. The role of the Reynolds stress term in equation (2) in dissipating wave growth is the object of the present study. The turbulent viscosity hypothesis is used to model the Reynolds stress which is the subject of section 4. The interfacial momentum contribution has components of drag, virtual mass, Basset force, turbulent diffusion and interfacial pressure. Most of the forces can be ignored based on their relative contributions. The virtual mass force is neglected based on the assumption of separated, stratified flow geometry. Only the component of drag is modelled as

$$M_{i1} = -\frac{1}{2H} C_D \rho_2 |u_1 - u_2| (u_1 - u_2) . \tag{3}$$

The drag coefficient is a power law correlation developed for wavy stratified flow [8]. The effect of interfacial pressure is not modelled with the other interfacial forces, but directly accounted for in the pressure gradient term. In traditional 1D models, the phasic pressures are assumed to be in equilibrium and the term appearing in (2) is the area averaged pressure. Instead, it is assumed here that the phases have distinct pressures that are related to a reference pressure with contributions from hydrostatic and surface tension forces, as shown in Figure 2.

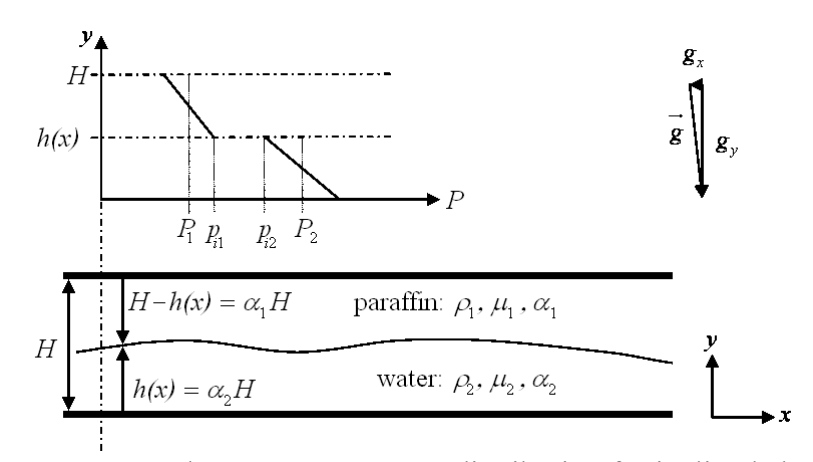


Figure 2 Geometry and transverse pressure distribution for inclined channel flow

The mean pressure of each phase can be related to its interfacial pressure by

$$P_k = p_{ik} \pm \frac{1}{2} H \rho_k g_y \alpha_k \tag{4}$$

$$(3/13)$$

for a rectangular channel. The pressure jump at the interface is proportional to the curvature of the interface which is approximated by the second derivative of the height of the interface. The interfacial pressure of the lighter fluid,  $p_{ig}$ , is selected as the reference pressure. Therefore, the mean pressure of the heavier phase is replaced by

$$P_2 = p_{i1} + \frac{1}{2}H\rho_2 g_y \alpha_2 - \sigma H \frac{\partial^2 \alpha_2}{\partial x^2} . \tag{5}$$

The four independent variables are  $\alpha_1$ ,  $u_1$ ,  $u_2$  and  $p_{i1}$ , with  $\alpha_2 = 1 - \alpha_1$ . In essence, this model is equivalent to the five equation two pressure model of Ramshaw and Trapp [2], incorporated into a single pressure framework.

## 3.1 Numerical implementation

The finite difference scheme of the governing equations is relatively simple. A staggered grid is used where velocities are stored at cell faces and void fraction, pressure, etc. are stored at the cell centroids. Only velocity is implicit in the continuity equation. The implicit velocity terms actually represent a velocity-pressure correction term. The continuity equations are solved implicitly for the void fraction and pressure in a coupled system and the momentum equations are solved explicitly for the velocity with updated pressure and void fraction corrections. The momentum convection is discretized with first order upwinding. Pressure, interfacial drag and the hydrostatic pressure force are modelled implicitly. Viscous shear is modelled with explicit second order central differencing. The third order derivative surface tension term is also explicit, second order and centered about the velocity face. face. This term requires two boundary conditions at the closed ends, which is satisfied by using two 'ghost' cells to extend the domain. These ghost cells mirror the calculated void fraction in the first or last cell. Both fluids are assumed to be incompressible.

## 3.2 Consequences of the model

Linear analyses and non-linear simulations of a 1D two-fluid model for stratified flow beyond the KH limit were performed [5]. The most important results are summarized below. The conditions used for the analysis are:  $\rho_2 = 1000 \text{ kg/m}^3$ ,  $\rho_1 = 780 \text{ kg/m}^3$ ,  $u_2 = 0.1 \text{ m/s}$ ,  $u_1 = 0.5 \text{ m/s}$ ,  $\alpha_1 = 0.5$ ,  $\sigma = 0.04 \text{ N/m}$ , H = 3 cm and the flow is horizontal,  $g_x = 0$ .

- The most basic 1D two-fluid model (i.e., neglecting interfacial drag, viscous stress, hydrostatic pressure and surface tension) is ill-posed when the relative velocity exceeds the inviscid Kelvin-Helmholtz instability criterion. As the wavelength of a disturbance decreases to zero, the growth rate increases to infinity.
- Interfacial drag has a stabilizing effect but does not alter the characteristics because the drag model is algebraic. The hydrostatic pressure force also has a slight stabilizing effect but does not change the ill-posed nature of the equations.
- Inclusion of a viscous stress term results in a finite growth rate for a zero wavelength disturbance [14]. Strictly speaking the model is well-posed, however the maximum growth rate occurs at the zero wavelength disturbance. This is physically incorrect because it is not infinitesimally small disturbances that dominate the observed wave growth. Additionally a

numerical model of this equation set would be non-convergent as the critical wavelength would be directly tied to the grid size.

- The model becomes fully well-posed, that is the growth rate of zero wavelength disturbances is zero, when a diffusion term is added to the continuity equation, but this is incorrect in terms of the two-fluid model. Incidentally, this is the reason why a first order upwind scheme stabilizes the two-fluid model. However, the numerical viscosity depends on the mesh size and the numerical model does not converge.
- When the third order surface tension term is considered the model becomes fully well-posed [2] for the right physical reason. There exists a cutoff wavelength (~1.8 cm) below which the growth rate is zero. The critical wavelength is approximately 2.5 cm.
- A Von Neumann stability analysis confirms the results of the dispersion analysis if the finite difference equations are consistent with the differential model. For the case with surface tension the cutoff wavelength is relatively unchanged and the critical wavelength is approximately 3 cm.
- Finally, a nonlinear simulation was carried out by solving the numerical model for a single wave with amplitude of 5% imposed on the baseline 0.5 void fraction. The growth of the wave was simulated over the first 200 iterations for different wavelengths confirming the previous analysis that the cutoff wavelength is approximately 2cm and the critical wavelength is shifted slightly to 4 cm.
- The results of a second hypothetical case are shown in Figure 3 where a short wavelength (1cm) disturbance of 0.5% amplitude is superimposed on a long wavelength (10 cm) disturbance of 5% amplitude. The high frequency wave is below the cutoff frequency predicted by the linear analysis. As predicted, Figure 3 clearly shows this wavelength is damped out while the large wave evolves. On the other hand, when surface tension is not included, the high frequency wave has a larger growth rate and dominates the solution. This is a good illustration of ill-posed behaviour.
- The long wavelength perturbation grows and begins to develop a steep, shock like formation. Wave growth is bounded by the viscous dissipation at the shock. So the role of the viscous stress is to stabilize the model in a non-linear sense.

Including the surface tension force into the 1D two-fluid model produced a system that is both more physically correct and well-posed. However, the model was found to have some shortcomings. The first problem that was noticed is that when the model is used to simulate the inclined channel experiment of Thorpe [6], the time of the onset of instability was significantly delayed from both the experimental data and the 2D simulations. Also the amplitude of the waves was significantly larger than the 2D model. It was determined that the first order nature of the finite difference equations made the model too stable if the interface was initially perfectly smooth. When a small amplitude disturbance in the void fraction was imposed, the initiation of wave growth matched the data. The most troublesome shortcoming of the model was its failure to converge on a solution as the mesh is refined. As the mesh size is reduced, higher frequency components of the solution appeared. It is hypothesized that the non-convergence issue and the large wave amplitude are both related to the fact that the dissipation is purely numerical. Although surface tension can make the model well-posed, it has a dispersive and not dissipative effect. There should be a dissipation mechanism in the model other than axial viscous dissipation that can retard the wave growth rate rather than relying on the numerical dissipation from the first order nature of the finite difference equations. In order to quantify the mechanism of dissipation by vorticity we rely on 2D CFD simulations of Thorpe's experiment [6].

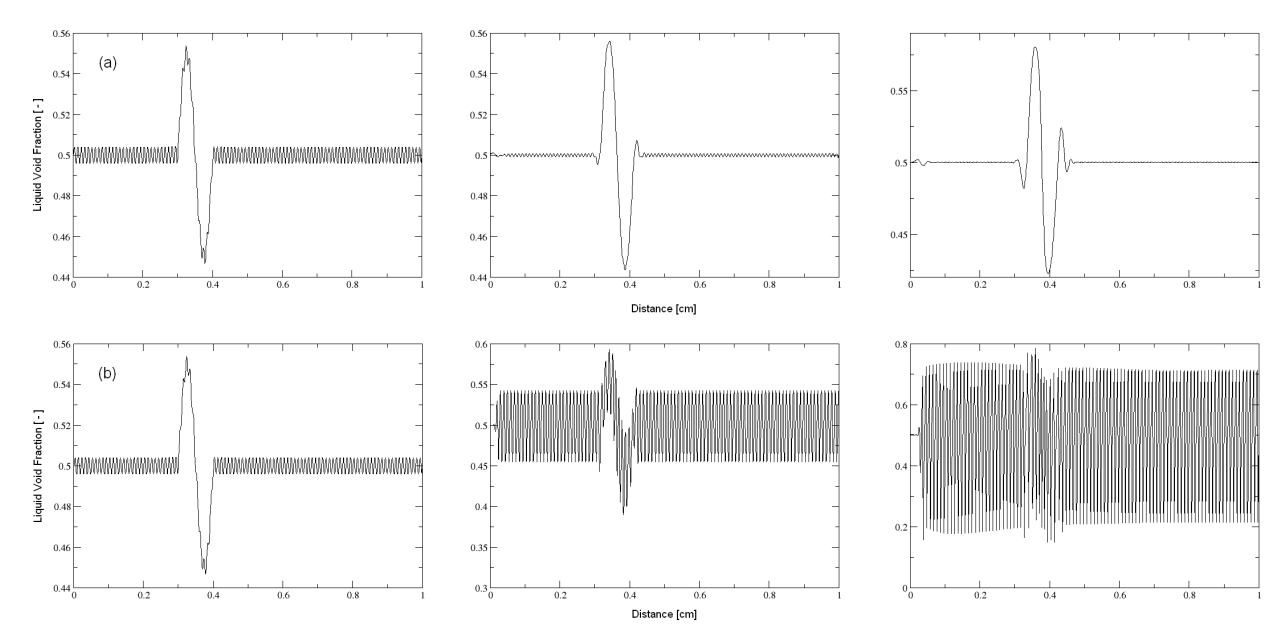


**Figure 3:** Evolution of a long and short wavelength disturbance with surface tension (a) and without (b), number of iterations are 0, 100, and 200 (left to right).

### 4. Two-dimensional CFD modelling

#### 4.1 Numerical model

The commercial code FLUENT is used to solve the incompressible, isothermal, 2D unsteady flow field. Due to the isothermal assumption the energy equation is not solved and mass transfer is hence neglected. The volume of fluid (VOF) approach is well suited to model the phase distribution of the two immiscible fluids. In this approach, it is assumed that a computational cell is occupied wholly by either phase or contains the interface. The velocity field is solved via a Large Eddy Simulation (LES). The justification for using an LES approach is given in section 4.2. The LES approach is not discussed in detail here, for reference see [10] or [11]. In general, the Navier-Stokes equations are filtered in either Fourier or physical space to remove the motion of small eddies below some cut-off or filter size. The subgrid scale stress (SGS), or eddy motion that has been filtered out, is modelled with the turbulent viscosity hypothesis. For the finite difference numerical implementation, the filtering is implicitly provided by the computational cell [11]. The governing equations are:

$$\sum_{k=1}^{2} \alpha_k = 1 \tag{6}$$

$$\frac{\partial}{\partial t}\alpha_1\rho_1 + \frac{\partial}{\partial x_i}\alpha_1\rho_1\overline{u}_i = 0 \tag{7}$$

$$\frac{\partial}{\partial t} \rho \overline{u}_i + \frac{\partial}{\partial x_j} \rho \overline{u}_i \overline{u}_j = -\frac{\partial \overline{p}}{\partial x_i} + \frac{\partial}{\partial x_j} 2\mu S_{ij} - \frac{\partial}{\partial x_j} \tau_{ij}^{SGS} + F_s$$
 (8)

where over-bars signify filtering. In (8) the density and viscosity are the void weighted average values if the interface is present in a cell. The only momentum force included in the analysis is surface tension force by using the continuum surface force [11]. The rate of strain tensor for the resolved scales is

$$\overline{S}_{ij} = \frac{1}{2} \left( \frac{\partial \overline{u}_i}{\partial x_j} + \frac{\partial \overline{u}_j}{\partial x_i} \right) \tag{9}$$

and the SGS is defined by and modelled as

$$\tau_{ij}^{SGS} \equiv \rho \overline{u_i u_j} - \rho \overline{u}_i \overline{u}_j = -2\mu_{SGS} \overline{S}_{ij}$$
 (10)

The SGS viscosity is determined with the Smagorinsky model [11] as

$$\mu_{SGS} = \rho C_s \overline{\Delta}^2 \left| \overline{S} \right| \tag{11}$$

where  $\overline{\Delta}$  is the grid filter length and  $|\overline{S}|$  is the modulus of the resolved rate of strain tensor, (9). The Smagorinsky constant  $C_s$  is determined dynamically. When the filtered equations are refiltered with a larger test filter, an expression for  $C_s$  can be derived based on a relationship between the grid scale filtered rate of strain and the test filtered rate of strain, see [10] or [11].

Time advancement of continuity, (7), is explicit for the purpose of using the highest accuracy representation of the interface. This is accomplished by the geometric reconstruction scheme, where the void fraction is assumed to vary linearly within each cell and uses this linear shape to calculate the advection of the fluids through the cell faces. The Pressure-Implicit with Splitting Operators (PISO) scheme is used for the pressure-velocity coupling. The spatial discrimination is second order bounded central difference with pressure staggering option (PRESTO!). Since the central difference scheme can be unstable, the time step is limited to ensure CFL < 1. Time advancement of the momentum equations is restricted to first order implicit. Ideally, second order accuracy is desired for LES but, unfortunately, that option is currently incompatible with explicit time advancement of the continuity equations (which is required for the high order accuracy interface treatment).

Currently only one computational grid is used where  $\Delta x = \Delta y = 1$ mm. In the future a convergence analysis will need to be performed. Here it is assumed that the mesh gives reasonably converged solution based on the work of [13] where Thorpe's case was studied with a VOF model and the same grid size was found to give a converged solution for the critical wavelength. All walls have no slip boundary conditions when the simulation is compared to Thorpe's data. Free slip conditions are used on the top and bottom walls to calculate the dissipation results. This was necessary to ensure that the calculated Reynolds stresses and dissipation were products of the wave motion and not from wall induced shear. The extra dissipation of the no slip walls at the ends of the channel does not affect the results due to the averaging domain discussed below. The initial condition is stagnant flow with the interface situated at the half channel height. The gravity vector points in the angle of channel tilt.

### 4.2 1D Reynolds stress

It is proposed to constitute a 1D Reynolds stress term that will produce the same amount of dissipation as the 2D Reynolds stresses obtained with LES. The 1D Reynolds stress should be constituted in terms of a turbulent viscosity and the covariance between the 2D and 1D strain rate tensors. The dissipation induced by turbulence will be accounted for by using the turbulent viscosity hypothesis [10] to relate the Reynolds stresses to the mean strain rate tensor. Ideally such a term would come directly from a simple Reynolds-averaged Navier-Stokes (RANS) formulation of the 2D model, (i.e. with either a k-e or k- $\omega$  type turbulence model). However it was observed that such an approach cannot be applied to Thorpe's case. RANS turbulence models developed for fully turbulent flow did not simulate accurately Thorpe's experiments because they are initially laminar and the turbulence in the shear layer never reaches a fully developed condition. Adding to the difficulty is the fact that the turbulence is initiated by the IKH instability. Therefore it was decided to perform an LES instead where the filtered. fluctuating velocity field is solved directly. Averaging of the fields to calculate the Reynolds stresses and the mean velocity gradients is necessary to 'back-calculate' the turbulent viscosity. Application of LES to quasi-2D seems counterintuitive due to the 3D nature of turbulence phenomena. However, it was verified independently by performing 2D LES of a single phase mixing layer (for which experimental turbulence data is readily available) that such an approach produces acceptable Reynolds stresses. Similar results for 2D LES of a mixing layer have also been obtained by Yang et. al. [12]

The space-time domain that is used to average the velocity fluctuations and the mean velocity gradients is  $x \in [0.6,1.2]$ m (the central one-third of the whole domain) and  $t \in [2.0,3.0]$ sec (after the formation of waves and before significant wave breaking). Averaging is performed for each time step along lines of constant y (Fig. 2) to obtain profiles for  $\langle \overline{u}' \overline{v}' \rangle$ ,  $\partial \langle \overline{u}_i \rangle / \partial x_j$  etc., with brackets signifying x-averages. The turbulent viscosity hypothesis

$$\left\langle \overline{u}'\overline{v}'\right\rangle = v_t \left( \frac{\partial \left\langle \overline{u}_i \right\rangle}{\partial x_j} + \frac{\partial \left\langle \overline{u}_j \right\rangle}{\partial x_i} \right) \tag{12}$$

is employed at each time step to obtain a y-dependent turbulent viscosity which is averaged to determine a value that can be implemented into the 1D model. The time history of the area averaged turbulent kinematic viscosity is shown in Figure 4a. Ideally the turbulent viscosity would scale with the area averaged relative velocity so that a model based on relative velocity as calculated by the 1D model could be implemented. Unfortunately it was determined that no such scale exists; therefore a constant turbulent viscosity is required. Ideally an asymptotic value could be selected, however for the present case the flow is continually developing. As the waves develop the viscosity increases until a point is reached where the wave breaking effect becomes more violent which disperses one phase into the other. In order to neglect this regime, the maximum turbulent viscosity from Figure 4 is selected, which is approximately  $v_t = 1.29 \cdot 10^{-5}$  m<sup>2</sup>s<sup>-1</sup>. Contributions of the SGS viscosity have not been transported into the 1D model because the *area averaged* values are lower than the molecular viscosity.

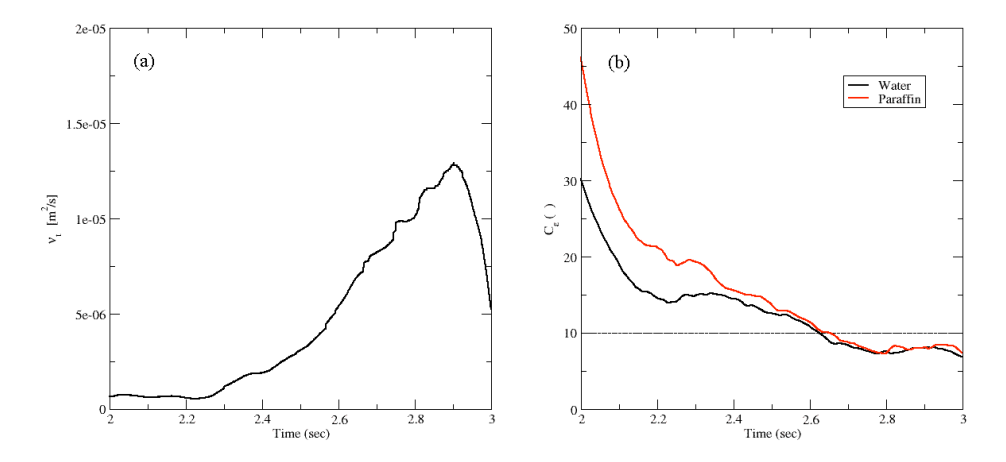


**Figure 4:** Turbulent viscosity (a) and 2D-1D dissipation (b) for use in the 1D model.

### 4.3 Dissipation covariance

Determining how to model the covariance term is equally as challenging due to shear stress being a tensor in 2D and a scalar in 1D. This is compounded by the fact that the axial diffusion is much smaller than the transverse components which do not exist in 1D. To remedy these challenges the total dissipation (sum of mean flow dissipation and turbulent dissipation)

$$\varepsilon = 2\nu \left\langle S_{ij} S_{ij} \right\rangle \tag{13}$$

is used, which is a scalar in any dimension. Then the dissipation covariance from 2D to 1D is

$$C_{\varepsilon} = \frac{\varepsilon_{i,j=1,2}}{\varepsilon_{i,j=1}} = \frac{\left\langle \left\langle 2\frac{\partial \overline{u}^{2}}{\partial x} + \frac{\partial \overline{v}^{2}}{\partial x} + 2\frac{\partial \overline{u}}{\partial y}\frac{\partial \overline{v}}{\partial x} + \frac{\partial \overline{u}^{2}}{\partial y} + 2\frac{\partial \overline{v}^{2}}{\partial y} \right\rangle \right\rangle}{\left\langle \left\langle 2\frac{\partial \overline{u}^{2}}{\partial x} \right\rangle \right\rangle}$$
(14)

where double brackets indicate x, and y averaging over the domain. Figure 4b shows the time history of (14) with void weighting over the calculated time. The constant covariance is chosen at the same instant that the turbulent viscosity was selected above, just over 2.9s. At this time the covariance is approximately 8.1 for both phases. Combining the results of (12) and (14) gives the effective viscosity that is used in (2):

$$\mu_{eff} = \rho_k C_{\epsilon} (v + v_t) \tag{15}$$

# 5. Comparison of 1D, 2D and data

The results of the 1D and 2D models are compared to the data in Figure 5 for four characteristic wave development stages. Note that these stages do not occur at the same time for each case. The 1D model exhibits wave growth to a point where sharp void gradients

similar to shocks appear on the windward side of the waves. These highly dissipative regions are responsible for limiting the growth in the 1D model (see Figure 4). The shock steepening and formation has been analysed by Kreiss and Ystrom [3]. Clearly the 2D results which show wave breaking and vortices are more physical. These vortices were identified experimentally by Banner and Phillips [15] who observed their formation on the forward face of the waves as the water tumbles forward without necessarily having discontinuities in the slope. Initially all of the vorticity is concentrated in a thin layer surrounding the interface as the phases accelerate counter-currently. As the KH instability develops and the waves break the vortex sheet stretches and folds resulting in a significant increase in viscous dissipation.

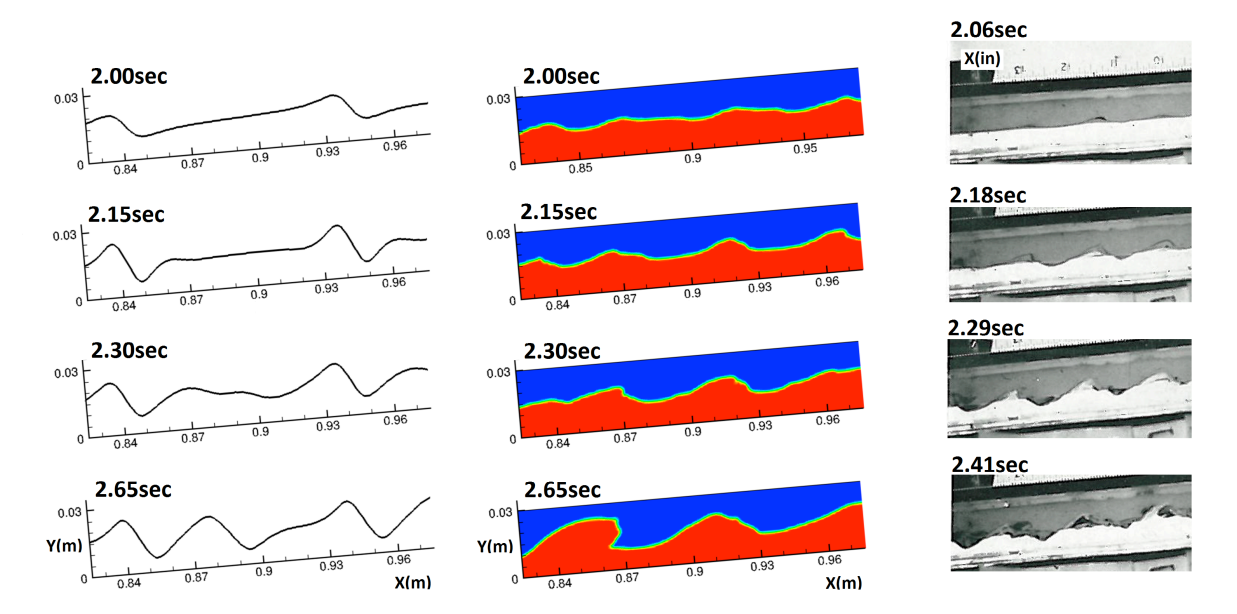


**Figure 5:** Water level profiles for the 1D, 2D models compared to the experimental data of Thorpe [6] (Permission granted by Cambridge University Press).

To compensate for the time lag in the onset of instability in the 1D model, a 10cm wavelength perturbation of amplitude 0.01 cm is imposed on the initial condition. This wave decays due to the initially subcritical relative velocity. However at a time of 1.7-1.8 sec this decay is halted and wave growth is observed. In the 2D model with an initially smooth interface, disturbances are first seen at 1.55 sec and wave growth is occurs at 1.8-1.9 sec. Both results agree well with the experimental observation of 1.88 sec.

The critical wavelength is measured by a fast Fourier transformation (FFT) of the interface location. In the 1D model, the FFT shows a single peak at 10 cm before the IKH transition due to the perturbed initial condition. After the onset of the instability, at 2.0 sec, there is a shift with the maximum wavelength being centred about 5 cm. There is also a secondary peak at 3 cm. Unfortunately the peak at 10 cm from the initial condition does not vanish. A short wavelength initial perturbation was tested in an attempt to destabilize to flow with a wave number outside of the range of interest. Such initial perturbations were completely damped out by the time of IKH. The FFT of the 2D interface shows a relatively broad 'peak' stretching from 2.5 to 4.5 cm at 2 sec, close to the onset. Later at 2.5 sec, a distinctive peak exists at 5.6cm. Both the 1D and 2D simulations slightly over predict the critical wavelength of the experimental data, 2.4 – 4.4 cm.

## 6. Convergence

Convergence was tested by using the effective viscosity for the sample problem of a single void wave in cocurrent channel flow. The geometry is the same as Thorpe's experiment and the relative velocity is 0.3m/s. It is clear from Figure 6a that without turbulent viscosity, only numerical viscosity plays a role and the model is non-convergent. As the mesh is refined higher and higher frequency components appear. This is due to the reduction in numerical viscosity and the dependence on the number of shocks to the inverse of viscosity [3]. Conversely Figure 6b shows that convergence can be reached when the numerical viscosity becomes insignificant compared to the turbulent viscosity. For the current implementation, when convergence is reached the smallest representable wavelength is 0.2 mm. mesh size Previously, it was shown that the cut off wavelength should be about 20 mm. This indicates that a higher order numerical method is required to bring the nonlinear cut off wavelength up to the scale predicted by the linear analysis.

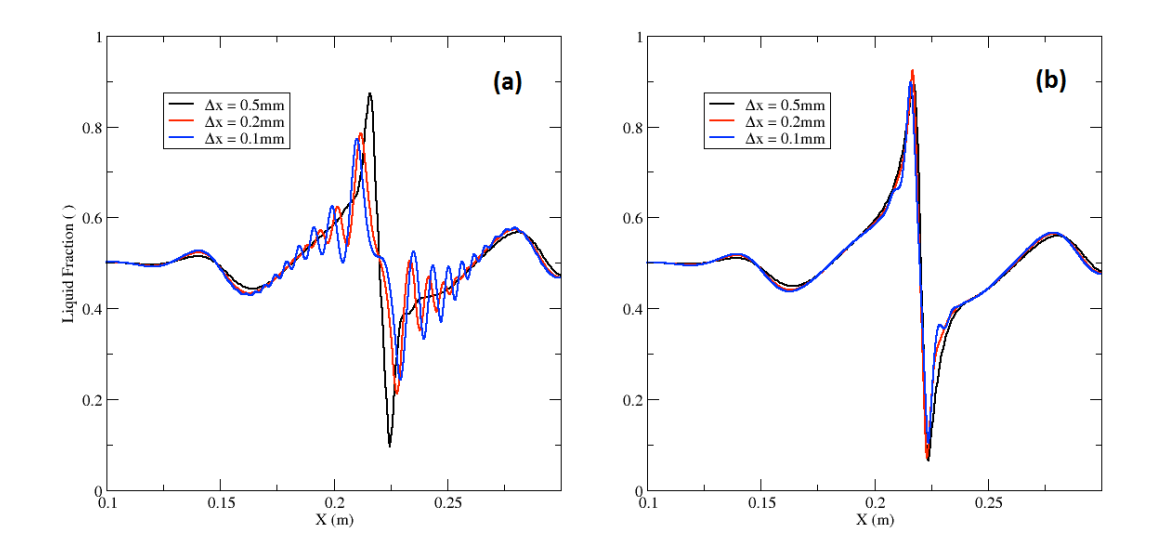


**Figure 6:** Evolution a single void wave for different meshes without considering Reynolds stresses (a) and with 5x the effective viscosity calculated for Thorpe's case (b).

#### 7. Conclusion

A non-linear stability analysis demonstrates the need of a Reynolds stress term in the 1D two-fluid model to limit the growth of the waves in case of a Kelvin-Helmholtz instability. In order to constitute a dissipative mechanism, a two-dimensional CFD analysis of Thorpe's experiment [6] was used to derive a turbulent viscosity and a dissipation covariance. The combination of these two results into an effective viscosity was used to model the physical mechanism of the Reynolds stress dissipation of turbulence in a 1D two-fluid model. It was shown that when a physical turbulent viscosity is used, instead of relying on numerical viscosity, the numerical model becomes convergent.

In practice a Reynolds stress is seldom included in 1D two-fluid models and numerical viscosity is used instead. Mathematically a physical viscous stress term is superior to numerical viscosity because numerical viscosity is mesh size dependent and the numerical model does not converge.

An important consequence of this non-linear stability analysis is that a viscous stress term is needed if a second or higher order numerical scheme is desired in cases where wave growth is expected (i.e., a high fidelity numerical 1D two-fluid model of a two-phase flow instability).

### 8. References

- [1] Y. Taitel, A. E. Dukler, "A model for prediction of flow regime transitions in horizontal and hear horizontal gas-liquid flow. AIChE J. Vol 22, 1976, pp 47 55.
- [2] J. D. Ramshaw and J. A. Trapp, "Characteristics, stability and short-wavelength phenomena in two-phase flow equation systems", Nucl. Sci. Eng., Vol 66, 1978, pp 93
- [3] K.-O. Kreiss and J. Ystrom, "A note on viscous conservation laws with complex characteristics", BIT Numer. Math., Vol 46, 2006, pp S55-S59.
- [4] R. Krishnamurthy and V. H. Ransom, "A non-linear stability study of the RELAP5/MOD3 two-phase model", <u>Proceedings of the Japan-US Seminar on Two-Phase Flow</u>, Berkeley, CA USA, 1992.
- [5] W. Fullmer, D. Prabhudharwadkar, A. Vaidheeswaran, V. H. Ransom and M. Lopez-de-Bertodano, "Linear and nonlinear analysis of the Kelvin-Helmholtz instability with the 1D two fluid model", <u>Proceedings of the 7<sup>th</sup> International Conference on Multiphase Flow</u>, Tampa, FL USA, May 30 June 4, 2010.
- [6] J. A. Thorpe, "Experiments on the instability of stratified shear flow: immiscible fluids", J. Fluid Mech. Vol 39, 1969, pp 25-48.
- [7] M. Ishii and T. Hibiki, Thermo-fluid dynamics of two-phase flow, Springer 2006.
- [8] J. E. Kowalski, "Wall and interfacial shear stress in stratified flow in a horizontal pipe", AIChE J. Vol. 33, No. 2, 1987, pp 274-281
- [9] H. Pokharna, M. Mori, and V. H. Ransom, "Regularization of two-phase flow models: a comparison of numerical and differential approaches", J. Comput. Phys., Vol 134, 1997, pp 282-295.
- [10] S. B. Pope, Turbulent flows, Cambridge University Press, 2009.
- [11] ANSYS FLUENT 12.0, Theory guide, April 2009.
- [12] W. B. Yang, H. Q. Zhang, C. K. Chan and W. Y. Lin, "Large eddy simulation of mixing layer", J. of Comp. and Applied Math. Vol 163, 2004, pp 311 318.
- [13] Y. Bartosiewicz, J. Lavieville, and J.-M. Seynhaeve, "A first assessment of the NEPTUNE\_CFD code: Instabilities in a stratified flow comparison between the VOF method and a two-field approach", Int. J. Heat and Fluid Flow, Vol 29, 2008, pp 460-478.
- [14] H. Holmas, T. Sira, M. NordsveenH.P. Langtangen, and R. Schulkes, "Analysis of a 1D incompressible two-fluid model including artificial diffusion" IMA J of Applied Math., Vol 73, 2008, pp 651-667.

Log Number: 256

[15] M.L. Banner and O. M. Phillips "Incipient breaking of small-scale waves" JFM, Vol 65, 1974, pp 647.